Nanoscale

High-Performance Electrolytic Oxygen Evolution with Seamless Armor Core-Shell FeCoNi Oxynitride

Journal:	*Nanoscale*
Manuscript ID	NR-COM-12-2018-010191.R1
Article Type:	Paper
Date Submitted by the Author:	06-Mar-2019
Complete List of Authors:	Di, Jun; Jiangsu University, School of Chemistry and Chemical Engineering; Nanyang Technological University, School of Materials Science and Engineering Zhu, Huiyuan ; Virginia Tech, Department of Chemical Engineering Xia, Jiexiang; Jiangsu University, School of Chemistry and Chemical Engineering Bao, Jian; Jiangsu University, Institute for Energy Research Zhang, Pengfei ; Oak Ridge National Laboratory, Chemical Sciences Division Yang, Shize; Oak Ridge National Laboratory, Materials Science Technology Division Li, Huaming; Jiangsu University Dai, Sheng; Oak Ridge National Laboratory,

High-Performance Electrolytic Oxygen Evolution with Seamless Armor Core-Shell FeCoNi Oxynitride

Jun Di,[a] Huiyuan Zhu,[d] Jiexiang Xia,[a,b] Jian Bao,[a] Pengfei Zhang,[b] Shi-Ze Yang,*[c] Huaming Li,[a] and Sheng Dai*[b]*

[a] School of Chemistry and Chemical Engineering, Institute for Energy Research, Jiangsu University, 301 Xuefu Road, Zhenjiang, 212013, P. R. China

[b] Chemical Sciences Division, Oak Ridge National Laboratory, Oak Ridge, USA

[c] Materials Science and Technology Division, Oak Ridge National Laboratory, USA

[d] Department of Chemical Engineering, Virginia Tech, Blacksburg, VA, USA

*Corresponding author

Abstract

Highly active, low-cost, and durable electrocatalysts for the water oxidation reaction are pivotal in energy conversion and storage schemes. Here we report the nitride-core, oxide-shell-armor structured FeCoNi oxynitride as an efficient oxygen evolution electrocatalyst with a homogeneously nitride ($Fe_{0.70}Co_{0.56}Ni_{0.92}N_{1.0}O_{0.06}$) core and oxide ($Fe_{0.48}Co_{0.1}Ni_{0.21}N_{0.05}O_{1.0}$) shell. The catalyst demonstrated an excellent activity for the oxygen evolution reaction with a current density of 10 mA cm^{-2} at a low overpotential of 0.291 V in alkaline media (1 M KOH), which is superior to the activities of commercial IrO_2, RuO_2, and Pt/C catalysts and comparable to state-of-the-art catalysts (e.g., NiFe-LDH, $NiCo_2O_4$, O-NiCoFe-LDH**)**. Density functional theory simulations suggested that the incorporation of multiple metal elements can indeed improve the reaction energetics with a synergistic effect from the core-shell structure. This unique structure of nitride-core with oxide-shell presents a new form of multimetallic oxyntride with compelling performance in electrolytic oxygen evolution.

Keywords: Oxygen evolution reaction; Electrocatalytic; Core-shell structure; Oxynitride; Synergistic effect

Ever-growing energy demand and growing carbon emissions have made it urgent to find alternatives to the traditional fossil fuels currently consumed in huge amounts.[1-4] Electrocatalytic water splitting is an appealing route to produce a renewable hydrogen energy source, which could simultaneously mitigate energy and environmental pollution problems.[5] Unfortunately, the efficiency of electrolytic water splitting is greatly limited to the sluggish kinetics of the multi-electron step involved in the oxygen evolution reaction (OER).[6-8] Even for the most efficient precious-metal catalysts such as ruthenium (Ru) and iridium (Ir) oxides,[9] a substantial overpotential is still required to acquire the desired current densities.[10] Therefore, designing and developing efficient electrocatalysts that are low in cost for the OER presents the grand challenge for the electrocatalytic water splitting process.

Transition-metal-based materials such as oxides,[11] hydroxides,[12] phosphates,[13] chalcogenides,[14] and perovskites[15] have been widely studied as potential alternative OER electrocatalysts owing to their earth-abundance, low cost, and environmental benignity. In particular, recent studies have found that metal nitrides, especially Ni_3N and Co_4N, can serve as efficient OER catalysts because of the outstanding electroconductivity enabled by their metallic-like features, potentially outperforming the well-studied metal oxide, hydroxide/phosphate systems.[16, 17] Nevertheless, these metal nitrides are thermodynamically less stable than metal oxides under oxidizing potentials, leading to the easy formation of passivation layers of oxides/hydroxides in oxidative aqueous environments.[17] This surface oxidation process has been confirmed on metal nitride catalysts during the OER process.[18] Therefore, the current transition-metal nitride systems still cannot meet the requirements for the OER necessary for them to be viably applied. Some recent studies have employed a binary system, including NiCo LDH [19] and $NiCo_2O_4$,[20] to promote OER catalysis. In this effort, we envision that Ni-Co bimetal nitrides with a homogeneous element dispersion and a protective shell might possess a synergistic effect, further promoting the OER performance.

More importantly, previous reports have shown that iron (Fe) can have an important modulating effect on nickel (Ni) or cobalt (Co) -based materials to increase the OER activity.[21, 22] The adsorption energy of OH, an important OER intermediate, is too weak on either Co-based or Ni-based material surfaces, and introducing Fe can promote the adsorption of OH.[10, 23] In addition, Fe is more vulnerable to oxidation than is Co or Ni and may serve as a sacrificed

species in the multimetallic structure with Ni and Co. Our strategy was to incorporate an Fe oxide armor layer on a nitride surface to boost the catalyst's stability for the OER. Once Fe is introduced to Ni-Co bimetal nitrides, the synergistic interplay among Fe, Co, and Ni will create a preferable local coordination environment and electronic structure that optimizes the adsorption energy of oxygenated species; at the same time, the Fe oxide armor shell will protect and maintain the integrity of the active Ni-Co nitride matrix.

Experimentally, FeCoNi oxynitride was synthesized by solvothermal and the gradient temperature control in particular atmosphere methods. Briefly, the multimetallic hydroxide precursor was firstly prepared and converted to oxynitride by nitridation. Based on the fact that the formation temperature of iron nitrides is higher than that of Ni and Co nitrides, here we employed a moderate temperature of 400^{o}C for the nitridation of the precursor to form Fe-doped Ni/Co nitrides and form oxides in situ on their surfaces. As a result, an armor-type nitride-core, oxide-shell (core-shell) structure was successfully constructed and demonstrated a largely enhanced OER activity compared with its single-metal or bimetal counterparts. The armor-type FeCoNi oxynitride materials afforded a current density of 10 mA cm^{-2} at a low overpotential of only 0.291 V, superior to those of commercial IrO_2, RuO_2, and Pt/C catalysts under identical experimental conditions, and comparable to or even better than the values for state-of-the-art catalysts.

The crystalline structures of the as-prepared FeCoNi oxynitride and the single-component counterparts were determined by x-ray diffraction (XRD) analysis. Pure Ni_3N and Co_2N were prepared via nitridation of the corresponding hydroxide precursors (**Figure 1, S1**); the peak of the Ni/Co bimetal nitride was more similar to that of Ni_3N (**Figure S1c**), which can be ascribed to the fact that Co entered into the crystal lattice of Ni_3N via doping. When Fe was introduced, the Ni_3N-like peak was also observed with additional Fe_3O_4 peaks (**Figure 1a**).

To characterize the electronic interactions within the FeCoNi oxynitride, x-ray photoelectron spectroscopy (XPS) measurements were acquired for the FeCoNi oxynitride material; the results are shown in **Figures 1b-d, S2**. The XPS results demonstrate the presence of the elements Fe, Co, Ni, N, and O in the FeCoNi oxynitride materials. Compared with Co_2N, the Co 2p3/2 and Co 2p1/2 peaks in the XPS spectrum of FeCoNi oxynitride were positively shifted by about 1.0 eV (**Figure 1b**). Compared with Ni_3N, the Ni 2p peak of FeCoNi oxynitride was

positively shifted by about 0.51 eV (**Figure 1c**). The N 1s peak in FeCoNi oxynitride displayed a positive shift (**Figure 1d**). These results suggest the existence of strong electronic interactions involving Fe, Co, and Ni tri-components in the FeCoNi oxynitride structure. The strong electronic interaction can be ascribed to the formation of a solid solution of an interior ternary metal.[24] Simultaneously, compared with a binary CoNi nitride, the Co 2p and Ni 2p peaks in FeCoNi oxynitride also display a shift (**Figure S3**), further revealing the strong electron interactions among the Fe, Co, and Ni tri-components in FeCoNi oxynitride. The XPS valence band spectra show that the introduction of Fe could change the surface valence band structure of the nitride, which could be important for oxygen adsorption during the electrocatalytic process (**Figure S4**).

The formation and morphology of the prepared FeCoNi oxynitride (**Figure 2a)** and single-component counterparts (**Figure S5 and S6**) were characterized by transmission electron microscopy (TEM) analysis. The single and binary nitrides show an irregular grain structure. **Figure 2b and 2c** clearly depict the FeCoNi oxynitride nanoparticle morphology with an average diameter of about 30 nm. In high-resolution bright field (BF) images (**Figure 2e**), a dark core can be clearly seen at the center of the nanoparticle and uniform lighter shell caps around it, suggesting the formation of a core-shell structure.[25] To further reveal the core-shell structure, high-resolution imaging was carried out. The clear boundaries in the core-shell structure can be clearly observed in **Figure 2f**. The thickness of the oxide shell is about 3 nm with a lattice spacing of around 0.298 nm, which agrees well with the crystallographic (220) spacing of Fe_3O_4, confirming the formation of an Fe oxide armor shell. The nitride-core structures are revealed in **Figure 2g**. A fast Fourier transform image (**inset Figure 2g**) shows the diffraction patterns corresponding to the [110] zone axis of the Me_3N structure with space group of p6322, which agrees with the XRD results. Co and Fe are more likely to be doped into the Ni_3N to form a solid solution–like nitride Me_3N structure in this core. Element mapping of FeCoNi oxynitride by electron energy loss spectroscopy (EELS) (**Figure 2d and Figure S7**) also shows a clear oxide shell and nitride core. To further determine the components of the nitride-core, oxide-shell structure, aberration-corrected scanning transmission electron microscope (STEM) with annular dark field (ADF) imaging and EELS measurements was carried out. A typical region with several core-shell nanoparticles is shown by ADF images in **Figure S8**. Although the shapes of particles vary considerably in the ADF images, they share the common characteristics of an

oxide shell and nitride core. The average chemical formulas of the nitride cores and oxide shells were determined to be $Fe_{0.70}Co_{0.56}Ni_{0.92}N_{1.0}O_{0.06}$ and $Fe_{0.48}Co_{0.1}Ni_{0.21}N_{0.05}O_{1.0}$, respectively (**Table S1 and S2**). The valence state of transition metals in the core and shell were analyzed using the L_3 to L_2 ratios in the EELS spectrum (**Figure S9**). The result shows that Fe, Co and Ni has a higher valence state in the shell than in the core (**Table S3**).

To investigate the OER catalytic performance of the obtained FeCoNi oxynitride catalysts, the samples were deposited onto glass carbon electrodes (0.284 mg cm^{-2}) and experiments were performed under a standard three-electrode system in 1.0 M KOH. In the polarization curves (**Figure 3a**), pristine Co_2N, and Ni_3N show a insignificant OER response. After the formation of Ni-Co bimetal nitride and introduction of Fe to the Co_2N or Ni_3N, the binary components displayed reduced onset potentials and higher current densities than their single-component counterparts. These results suggest that building a Ni-Co bimetal nitride or Fe modification can improve the catalytic activity. Futhermore, the tri-metal FeCoNi oxynitride showed even better performance. Intriguingly, FeCoNi oxynitride displayed an initial O_2 evolution at a very small overpotential of 0.23 V, much smaller than that of binary FeNi (0.29 V), binary CoNi (0.32), and binary FeCo (0.34 V). For comparison, commercial IrO_2, RuO_2, and Pt/C (20 wt % platinum on Vulcan carbon black) were also investigated under the same conditions (**Figure 3b**). Noticeably, the onset potential of FeCoNi oxynitride was also much lower than that of IrO_2, RuO_2, and Pt/C, and the OER current density of FeCoNi oxynitride even exceeded that of commercial catalysts. By comparing the current density at a potential of 0.57 V vs. Ag/AgCl, it was found that under the same conditions, FeCoNi oxynitride displayed a current density of 47.16 mA cm^{-2}, much higher than that of Co_2N, Ni_3N, binary FeCo, binary CoNi, or binary FeNi (**Figure 3c**). The current density acquired from FeCoNi oxynitride was roughly 4.29, 5.07, and 23.35 times higher than the densities of commercial Ir-C, RuO_2, and IrO_2, respectively, at 1.56 V vs RHE.

The current density value of 10 mA cm^{-2} is particularly important because it is the current density of a device with 10% solar-to-hydrogen conversion under 1-sun illumination.[26] The overpotential (η) required to achieve a 10 mA cm^{-2} current density was determined, and the result is shown in **Figure 3d**. FeCoNi oxynitride displayed a required overpotential of 0.291 V, exhibiting a lower required overpotential than Co_2N (0.413 V), Ni_3N (0.388 V), binary FeCo (0.371 V), binary CoNi (0.366 V), and binary FeNi (0.350 V). Considering the similar BET specific surface area of the samples, the law of obtained normalized intrinsic activity of catalysts

still match the original result, thus the improved OER performance of FeCoNi oxynitride may not be derived from the difference in specific surface area (**Figure S10, S11**). At the same time, the required overpotential of 0.291 V was also much lower than those of commercial Ir-C, RuO_2, and IrO_2. This overpotential places the FeCoNi oxynitride catalyst among the top tier of water oxidation catalysts in alkaline media, outperforming NiFe-LDH single-layer nanosheets (0.302 V),[19] monolayer $Ni_{0.75}V_{0.25}$-LDH (0.318 V),[27] $NiCo_2O_4$ ultrathin nanosheets (0.320 V),[28] CoMnP nanoparticles (0.330 V),[29] $Co_3O_4/NiCo_2O_4$ double-shelled nanocages (0.340 V),[30] Ni-Co mixed oxide cages (0.380 V),[31] O-NiCoFe-LDH (0.420 V),[32] single-crystal Co_3O_4@CoO (0.430 V),[33] and others (**Table S4**). These results are further evidence of the advantages of the novel FeCoNi oxynitride core-shell materials.

By compensating the raw data with the iR losses, the OER behavior of FeCoNi oxynitride was found to be even more impressive (**Figure 4a**). At the same time, the OER performance of FeCoNi oxynitride was further measured in a lower-alkalinity solution (0.1 M KOH) because some devices, such as metal-air batteries, often perform better in less basic solutions. Generally, a higher overpotential was required for the OER in the less-basic solution. It is desirable to develop an OER catalyst with lower overpotential losses in less-basic solutions. As shown in **Figure 4a**, the required overpotential to achieve a 10 mA cm^{-2} current density was about 0.326 V, which also revealed an advantage for FeCoNi oxynitride compared with state-of-the-art OER catalysts in a lower-alkalinity electrolyzer (**Table S4**). This finding further demonstrates the superiority of the FeCoNi oxynitride catalysts. The Tafel slope of FeCoNi oxynitride (63.8 mV/decade) was lower than that of IrO_2 (87.3 mV/decade), RuO_2 (136.1 mV/decade), and Pt/C (174.7 mV/decade), revealing its superior reaction kinetics (**Figure 4b**). To further assess the OER catalytic ability, the turnover frequency (TOF) of the obtained catalysts at η of 0.35 V is presented here (**Figure 4c**). We found that FeCoNi oxynitride displayed the highest TOF of $\sim 2.49 \times 10^{-2}$ s^{-1}, which was ~13.9 and ~10.6 times higher than those of Co_2N and Ni_3N, respectively. The superior OER activity of FeCoNi oxynitride can be attributed to the synergistic effects of the core-shell structures. The strong electronic interactions provided reliable electronic transmission, which enabled the high electrical conductivity of FeCoNi oxynitride efficiently (**Figure S12**). Apart from OER activity, durability is another important factor in the appraisal of an advanced catalyst. EELS elemental mapping of FeCoNi oxynitride after cycling was performed (**Figure S13**). Compared with the initial FeCoNi oxynitride, the core-shell structure

was maintained with homogeneously dispersed nitride as core and oxide as shell, demonstrating the excellent durability of FeCoNi oxynitride materials. After stability test, the chemical formula of the core-shell structure became $Fe_{1.31}Co_{1.82}Ni_{3.51}N_{1.0}O_{0.0}$ for the core and $Fe_{0.64}Co_{0.31}Ni_{0.38}N_{0.0}O_{1.0}$ for the shell (**Figure S14**). After cycling, the valence state of Fe increased in both core and shell. It is interesting to notice that the valence state of Co is higher in the shell than in the core after the reaction. The valence state of Ni remained nearly the same after reaction (**Table S3**). The XRD is performed on the used FeCoNi oxynitride sample, as shown in **Figure S15**. The crystal structures of the FeCoNi oxynitride sample do not change greatly after cycle, which clearly suggests that the FeCoNi oxynitride materials are stable during the OER process. As shown in **Figure 4d**, after 1000 cycles, the polarization curve for FeCoNi oxynitride displayed an onset potential similar to the initial potential, with a slightly positive shift to a higher potential. This is further evidence of the excellent durability of the FeCoNi oxynitride electrocatalyst with a core-shell structure. High-temperature hydrogenation was performed to treat the FeCoNi oxynitride, and the oxide shell was destroyed (**Figure S16**). Significantly deteriorated OER behavior was observed after 30 cycles (**Figure S17**), which is further evidence of the significance of the oxide shells.

Density functional theory simulations were carried out to gain a deeper understanding of the structural effect on the OER. We compared four different surface structures, including an Ni_3N surface, Ni_3N doped with Fe and Co, an Fe_3O_4 surface, and an Fe_3O_4 surface doped with Ni and Co. The free energy diagram of the OER with four electrons, shown in **Figure 5a**, was calculated as described in the supplementary information part. It was found that metallic Ni_3N and Ni_3N alloy surfaces generally had very large energy barriers for the OOH* formation step. The alloy effect was very small in the Ni_3N structure. In the oxide structure, doping with Ni and Co improved the reaction energetics. With the formation of the nitride/oxide core-shell structure, the reaction energetics might be further tuned to the in-between regions toward optimal energies. The binding energies of different intermediate species are shown in **Figure 5b**. Generally, metallic nitride structures bind the intermediate species stronger than oxides do, and the binding energies vary with doping. Those results indicate that the nitride-core, oxide-shell structure would provide favorable energetic pathways for the OER, which explains the excellent performance in experiments.

The superior catalytic performance of core-shell structured FeCoNi oxynitride in the OER can be attributed to the synergistic effects of the homogeneously dispersed multivariant components and unique core-shell structure. First, the metallic-phase nitride core ensures the excellent electrical conductivity of the FeCoNi oxynitride electrocatalyst. Second, according to previous reports, the adsorption energy of OH is too strong on an Fe-based material surface and too weak on Co-based and Ni-based material surfaces.[10, 23] The synergistic interplay between Fe, Co, and Ni produced a favorable local coordination environment and electronic structure that optimized the adsorption energy and improved the OER behavior. Third, the oxide shell effectively prevented electrode corrosion and enabled the high OER stability. These unique advantages significantly promoted the reaction kinetics and enhanced the stability of this earth-abundant FeCoNi oxynitride catalyst for the OER.

Conclusions

In summary, we successfully developed a novel core-shell structure FeCoNi oxynitride, with nitride $Fe_{0.70}Co_{0.56}Ni_{0.92}N_{1.0}O_{0.06}$ as the core and oxide $Fe_{0.48}Co_{0.1}Ni_{0.21}N_{0.05}O_{1.0}$ as the shell, as an extraordinary OER catalyst in alkaline media. FeCoNi oxynitride catalysts displayed a greatly reduced onset potential and higher current density than their single- or dual-component counterparts. The unique core-shell architectures with Fe, Co, or Ni ternary metal components homogeneously dispersed in the nitride core enabled a synergistic effect for the OER process, and the oxide shell endowed FeCoNi oxynitride with high stability. The strategy of employing a multimetallic component to improve catalytic activity and a protective shell to enhance catalytic stability should be broadly applicable to a range of important reactions involved in next-generation of energy conversion and storage schemes. The novel material also displayed performance comparable to or superior to that of a state-of-the-art catalyst.

Corresponding Authors:
*E-mail: xjx@ujs.edu.cn, ananyjlo@gmail.com, dais@ornl.gov

Notes
The authors declare no competing financial interest.

Acknowledgements

This work was financially supported by the National Natural Science Foundation of China (Nos. 21676128, 21576123, 21476098 and 21471069). S.D. and H.Z. were sponsored by the Division of Chemical Sciences, Geosciences, and Biosciences, Office of Basic Energy Sciences, US Department of Energy. The electron microscopy at Oak Ridge National Laboratory (S.Z.Y.) was supported by the US Department of Energy, Office of Science, Basic Energy Sciences, Materials Sciences and Engineering Division, and was performed in part as a user proposal at the Oak Ridge National Laboratory Center for Nanophase Materials Sciences, which is a DOE Office of Science User Facility.

References

[1] C. Niether, S. Faure, A. Bordet, J. Deseure, M. Chatenet, J. Carrey, B. Chaudret and A. Rouet, *Nat. Energy,* 2018, **3**, 476-483.

[2] M. Sun, H. J. Liu, Y. Liu, J. H. Qu and J. H. Li, *Nanoscale*, 2015, **7**, 1250-1269.

[3] M. Sun, D. Davenport, H. J. Liu, J. H. Qu, M. Elimelech and J. H. Li, *J. Mater. Chem. A*, 2018, **6**, 2527-2539.

[4] M. Sun, G. Zhang, H. J. Liu, Y. Liu and J. H. Li, *Sci. China Mater.*, 2015, **58**, 683-692.

[5] J. S. Luo, J. H. Im, M. T. Mayer, M. Schreier, M. K. Nazeeruddin, N. G. Park, S. D. Tilley, H. J. Fan and M. Grätzel, *Science,* 2014, **345**, 1593-1596.

[6] X. J. Zhao, P. Pachfule, S. Li, J. R. J. Simke, J. Schmidt and A. Thomas, *Angew. Chem. Int. Ed.,* 2018, **57**, 8921-8926.

[7] M. Sun, H. J. Liu, J. H. Qu and J. H. Li, *Adv. Energy Mater.*, 2016, **6**, 1600087.

[8] G. Zhang, G. C. Wang, Y. Liu, H. J. Liu, J. H. Qu and J. H. Li, *J. Am. Chem. Soc.*, 2016, **138**, 14686-14693.

[9] M. R. Gao, W. C. Sheng, Z. B. Zhuang, Q. R. Fang, S. Gu, J. Jiang and Y. S. Yan, *J. Am. Chem. Soc.,* 2014, **136**, 7077-7084.

[10] B. Zhang, X. L. Zheng, O. Voznyy, R. Comin, M. Bajdich, M. García-Melchor, L. L. Han, J. X. Xu, M. Liu, L. R. Zheng, F. P. G. de Arquer, C. T. Dinh, F. J. Fan, M. J. Yuan, E. Yassitepe, N. Chen, T. Regier, P. F. Liu, Y. H. Li, P. De Luna, A. Janmohamed, H. L. L. Xin, H. G. Yang, A. Vojvodic and E. H. Sargent, *Science,* 2016, **352**, 333-337.

[11] R. D. L. Smith, M. S. Prévot, R. D. Fagan, Z. P. Zhang, P. A. Sedach, M. K. J. Siu, S. Trudel and C. P. Berlinguette, *Science,* 2013, **340**, 60-63.

[12] M. Gong, Y. G. Li, H. L. Wang, Y. Y. Liang, J. Z. Wu, J. G. Zhou, J. Wang, T. Regier, F. Wei and H. J. Dai, *J. Am. Chem. Soc.,* 2013, **135**, 8452-8455.

[13] Y. Yang, H. L. Fei, G. D. Ruan and J. M. Tour, *Adv. Mater.,* 2015, **27**, 3175-3180.

[14] S. Dou, L. Tao, J. Huo, S. Y. Wang and L. M. Dai, *Energy Environ. Sci.,* 2016, **9**, 1320-1326.

[15] J. Suntivich, K. J. May, H. A. Gasteiger, J. B. Goodenough and Y. Shao-Horn, *Science,* 2011, **334**, 1383-1385.

[16] K. Xu, P. Z. Chen, X. L. Li, Y. Tong, H. Ding, X. J. Wu, W. S. Chu, Z. M. Peng, C. Z. Wu and Y. Xie, *J. Am. Chem. Soc.,* 2015, **137**, 4119-4125.

[17] P. Z. Chen, K. Xu, Z. W. Fang, Y. Tong, J. C. Wu, X. L. Lu, X. Peng, H. Ding, C. Z. Wu and Y. Xie, *Angew. Chem. Int. Ed.,* 2015, **54**, 14710-14714.

[18] S. Jing, *ACS Energy Lett.,* 2017, **2**, 1937-1938.

[19] F. Song and X. L. Hu, *Nat. Commun.,* 2014, **5**, 4477.

[20] X. H. Gao, H. X. Zhang, Q. G. Li, X. G. Yu, Z. L. Hong, X. W. Zhang, C. D. Liang and Z. Lin, *Angew. Chem. Int. Ed.,* 2016, **55**, 6290-6294.

[21] L. Trotochaud, S. L. Young, J. K. Ranney and S. W. Boettcher, *J. Am. Chem. Soc.,* 2014, **136**, 6744-6753.

[22] M. S. Burke, M. G. Kast, L. Trotochaud, A. M. Smith and S. W. Boettcher, *J. Am. Chem. Soc.,* 2015, **137**, 3638-3648.

[23] J. Zhang, T. Wang, D. Pohl, B. Rellinghaus, R. H. Dong, S. H. Liu, X. D. Zhuang and X. L. Feng, *Angew. Chem. Int. Ed.,* 2016, **55**, 6702-6707.

[24] J. X. Feng, H. Xu, Y. T. Dong, S. H. Ye, Y. X. Tong and G. R. Li, *Angew. Chem. Int. Ed.,* 2016, **55**, 3694-3698.

[25] Z. B. Zhuang, W. C. Sheng and Y. S. Yan, *Adv. Mater.,* 2014, **26**, 3950-3955.

[26] C. C. L. McCrory, S. Jung, I. M. Ferrer, S. M. Chatman, J. C. Peters, T. F. Jaramillo, *J. Am. Chem. Soc.,* 2015, **137**, 4347-4357.

[27] K. Fan, H. Chen, Y. F. Ji, H. Huang, P. M. Claesson, Q. Daniel, B. Philippe, H. K. Rensmo, F. S. Li, Y. Luo and L. C. Sun, *Nat. Commun.,* 2016, **7**, 11981.

[28] J. Bao, X. D. Zhang, B. Fan, J. J. Zhang, M. Zhou, W. L. Yang, X. Hu, H. Wang, B. C. Pan and Y. Xie, *Angew. Chem. Int. Ed.,* 2015, **54**, 7399-7404.

[29] D. Li, H. Baydoun, C. N. Verani and S. L. Brock, *J. Am. Chem. Soc.,* 2016, **138**, 4006-4009.

[30] H. Hu, B. Y. Guan, B. Y. Xia and X. W. Lou, *J. Am. Chem. Soc.,* 2015, **137**, 5590-5595.

[31] L. Han, X. Y. Yu and X. W. Lou, *Adv. Mater.,* 2016, **28**, 4601-4605.

[32] L. Qian, Z. Y. Lu, T. H. Xu, X. C. Wu, Y. Tian, Y. P. Li, Z. Y. Huo, X. M. Sun and X. Duan, *Adv. Energy Mater.,* 2015, **5**, 1500245.

[33] C. W. Tung, Y. Y. Hsu, Y. P. Shen, Y. X. Zheng, T. S. Chan, H. S. Sheu, Y. C. Cheng and H. M. Chen, *Nat. Commun.,* 2015, **6**, 8106.

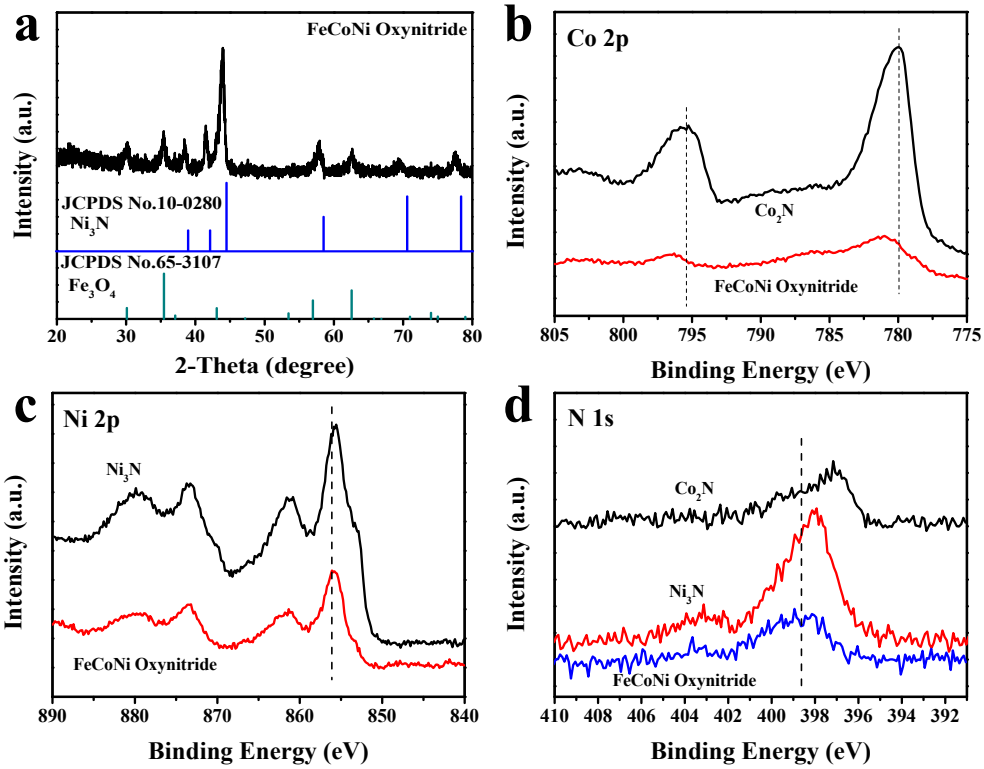

Figure 1. (a) XRD patterns for FeCoNi oxynitride; XPS spectra of (b) Co 2p, (c) Ni 2p, (d) N 1s for FeCoNi oxynitride, Co_2N, and Ni_3N.

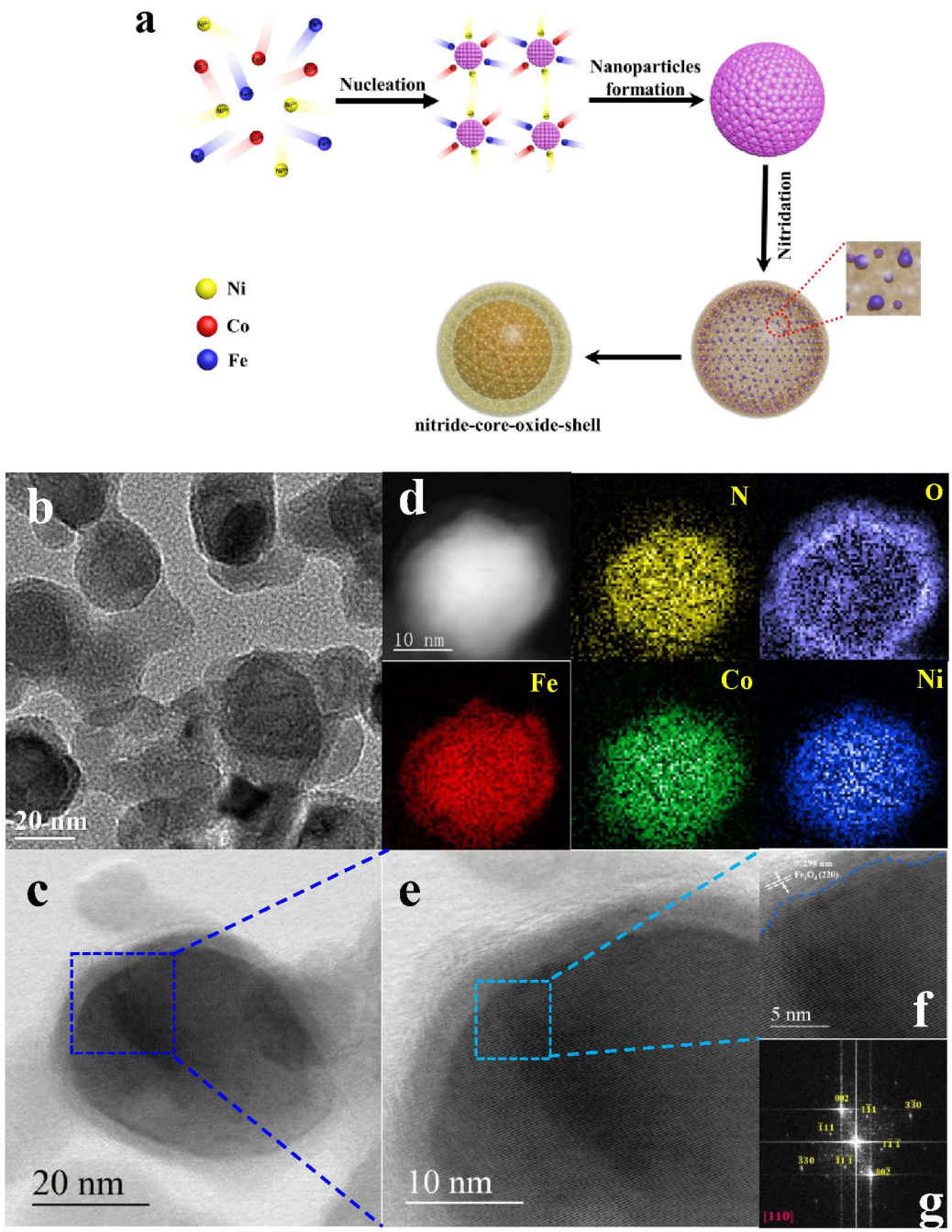

Figure 2. (a) Illustration of the formation of nitride-core, oxide-shell FeCoNi oxynitride nanoparticles. STEM study of core-shell particles. (b) TEM image of nitride-core, oxide-shell FeCoNi oxynitride nanoparticles. (c) Higher-magnification STEM-BF images. (d) The corresponding EELS elemental mappings. (e) BF image of blue upper region of the particle. (f)

BF image showing the core-shell interface. (g) Fast Fourier transform of image c showing diffraction patterns along the [110] zone axes of nickel-cobalt-iron alloy nitrides (Me_3N).

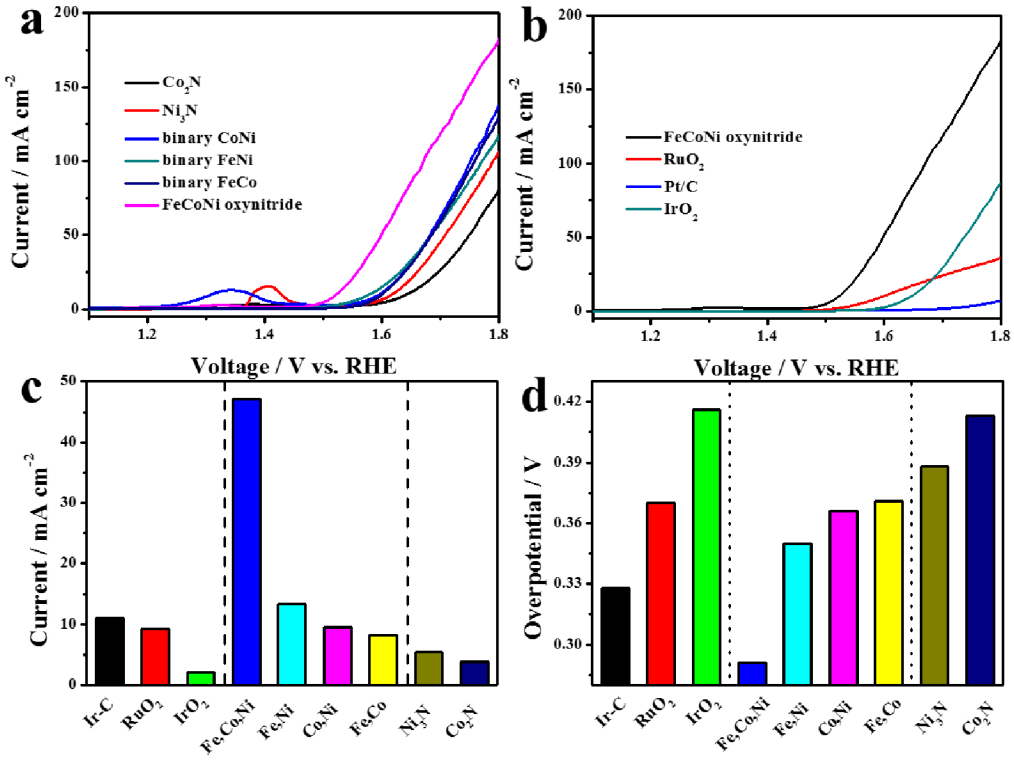

Figure 3. (a) Polarization curves of FeCoNi oxynitride, binary FeCo, binary FeNi, binary CoNi, Co_2N, and Ni_3N samples for OER at a scan rate of 5 mV/s (1M KOH, without *iR* correction). (b) Polarization curves of the commercial IrO_2, RuO_2, and Pt/C. (c) Comparison of the current achieved at a potential of 1.6 V vs. RHE (reversible hydrogen electrode). (d) The overpotential required for a current density of 10 mA cm^{-2} (without *iR* correction) and an Ir/C (20 wt %) catalyst as a reference.[12, 28]

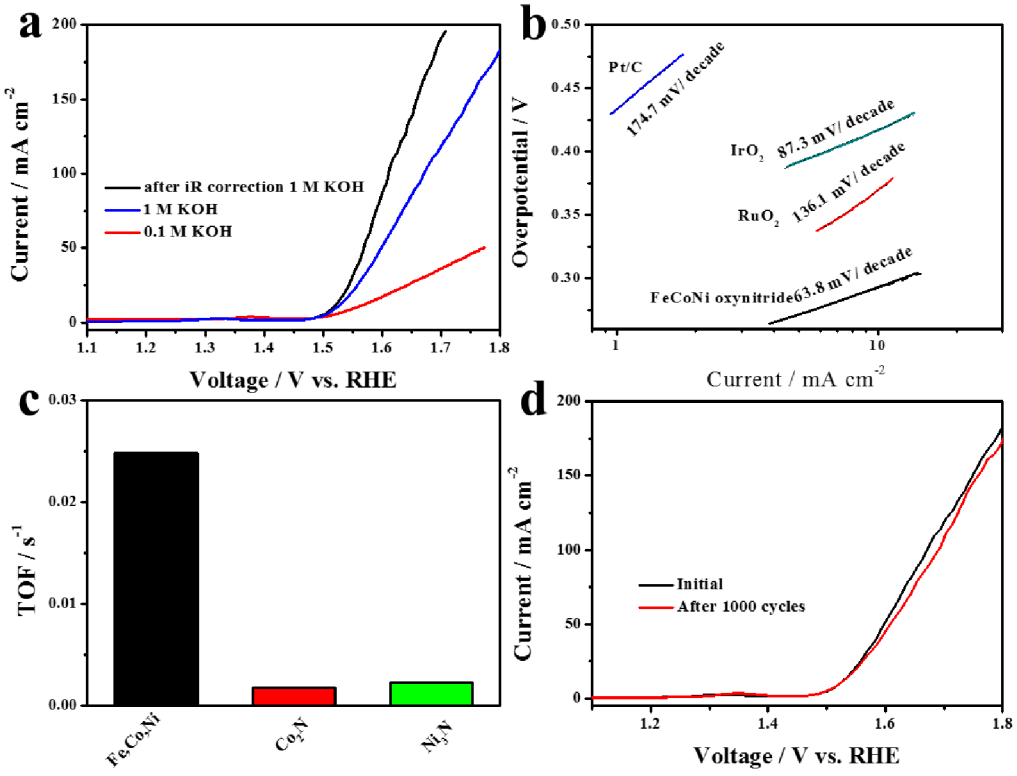

Figure 4. (a) Comparison of the linear sweep voltammetry (LSV) curves of FeCoNi oxynitride with or without *iR* correction and an LSV curve measured in 0.1M KOH (without *iR* correction). (b) Tafel plots of the samples. (c) TOF values calculated from the current at η = 0.35 V. (d) Polarization curves after 1000 CV cycles with the FeCoNi oxynitride electrode.

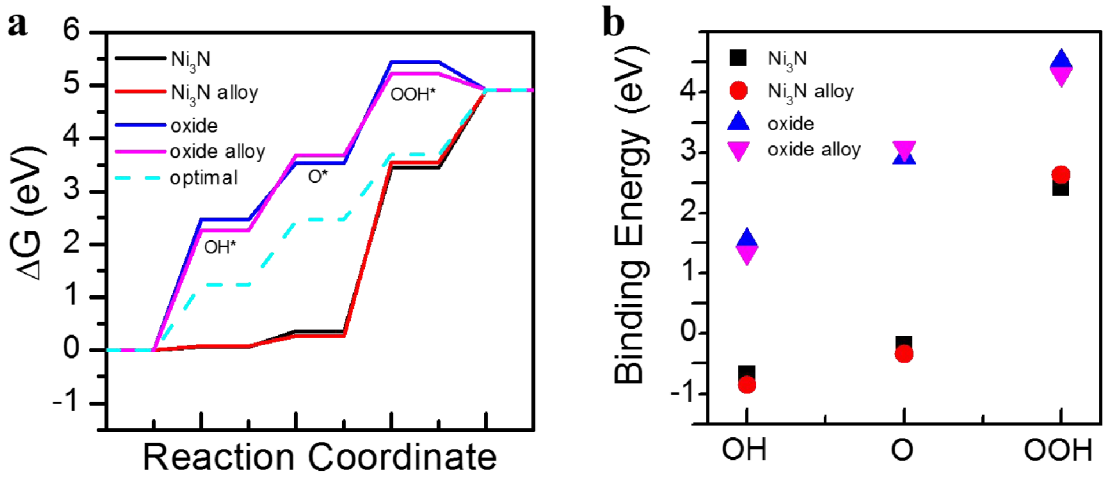

Figure 5. (a) Free energy diagram of different intermediate species on different surfaces; (b) binding energies of intermediate species on different surfaces.

TOC